Journal of Catalysis **211,** 496–510 (2002)
doi:10.1006/jcat.2002.3748

Performance and Kinetic Behavior of a New SiO_2-Attached Molecular-Imprinting Rh-Dimer Catalyst in Size- and Shape-Selective Hydrogenation of Alkenes

Mizuki Tada, Takehiko Sasaki, and Yasuhiro Iwasawa[1]

Department of Chemistry, Graduate School of Science, The University of Tokyo Hongo, Bunkyo-ku, Tokyo, 113-0033, Japan

Received April 29, 2002; revised July 4, 2002; accepted July 11, 2002

A new size- and shape-selective Rh-dimer catalyst was designed by combination of a metal-complex-attaching method and a molecular-imprinting method on an Ox.50 surface. Coordinatively unsaturated, air-stable Rh dimers with a Rh–Rh bond of 0.268 nm were prepared in 0.74-nm micropores of SiO_2-matrix overlayers on the Ox.50 silica surface by attaching a $Rh_2Cl_2(CO)_4$ precursor on the surface ($Rh_2Cl_2(CO)_4/SiO_2$), followed by coordination of template ligands $P(OCH_3)_3$ to the attached Rh species (Rh_{sup} catalyst), and then by surface imprinting of the template with SiO_2-matrix overlayers formed by hydrolysis–polymerization of $Si(OCH_3)_4$ (Rh_{imp} catalyst). The Rh dimers, micropores, and SiO_2-matrix overlayers in the molecular-imprinting Rh_{imp} catalyst were characterized by EXAFS, BET analysis, and ^{29}Si solid-state MAS NMR, respectively. It was found that activity of the Rh_{sup} catalyst for hydrogenation of alkenes was promoted remarkably (35–51 times) after the imprinting. The alkene hydrogenation proceeded on the imprinted Rh dimers with a monohydride without any breaking of the Rh–Rh bond. Size and shape selectivities of the molecular-imprinting Rh_{imp} catalyst were examined by measuring the hydrogenation rates of eight alkenes of different sizes and shapes. It was also found that the Rh_{imp} catalyst exhibited not only high activity and stability but also size and shape selectivities for the alkene molecules, probably due to a template-size cavity, created behind the removed template ligand, being used as a reaction site. Activation energies and activation entropies for the hydrogenation of large and branched alkenes were much smaller than those for small alkenes, which implies a shift in the rate-determining step in the reaction sequence for alkene hydrogenation. The performance of the molecular-imprinting Rh-dimer catalyst is discussed from structural and kinetic viewpoints.

Key Words: **molecular imprinting; supported metal complex; template; micropores; Rh-dimer catalyst; hydrogenation of alkenes; EXAFS; size selectivity; shape selectivity.**

INTRODUCTION

The regulation of catalytic reactions to produce desired products preferentially has long been challenged from both fundamental and industrial interests. In native systems, antibodies and enzymes act as highly selective catalysts for various reactions under mild reaction conditions, and artificial synthesis of such active and selective catalysts is one of the attractive subjects in catalytic chemistry. Recently, molecular-imprinting materials possessing cavities of template-molecular shapes have been prepared (1–9) and used for many processes, such as that of receptor (10–12), chromatographic separation (13, 14), chemical sensing (15–18), and catalysis (19–28). Molecular imprinting is a promising approach to the preparation of artificial enzymatic catalysts. However, there have been few attempts at the molecular imprinting of metal complexes, though many important catalytic reactions proceed on metal sites (29–34).

Bulk imprinting of metal complexes has been utilized to stabilize labile metal complexes (35, 36), to bind selectively particular ligands at the metal sites (37), and to prepare selective catalysts (29–34) for, e.g., Diels–Alder reaction on Ti complex (30), hydrogenation of ketones on Rh catalyst (31), hydride transfer reduction of prochiral ketones on Ru and Rh complexes (32, 33), and so forth. In these cases of imprinting by bulk polymer matrices, however, slow diffusion of reactant molecules causes a decrease in catalytic activity because of disadvantageous locations of catalytic sites in bulk polymers. Further, distribution of pores produced in the polymer matrices is often nonuniform and ill defined (37), which is a fatal problem for selectivity. The difficulty of characterizing the imprinted sites in bulk matrices has prevented demonstration of the mechanism in regulating catalytic reactions at the imprinted sites.

On the other hand, imprinting at oxide surfaces can provide catalytic sites that are readily accessible to reactant molecules, located in template pores of matrices deposited on the surfaces. The obtained samples were employed as efficient catalysts for alkene combustion and amide hydrolysis reactions (38, 39). However, to our knowledge, there is no example of successful molecular imprinting of metal complexes at oxide surfaces for catalyst design thus far. Hence, it is a challenging project, designing imprinted metal

[1] To whom correspondence should be addressed. Fax: 81-3-5800-6892. E-mail: iwasawa@chem.s.u-tokyo.ac.jp.

0021-9517/02 $35.00

complexes which are chemically attached on oxide surfaces and surrounded by matrix overlayers on the surfaces. We have demonstrated that metal complexes attached on oxide surfaces exhibit unique catalytic properties, which are much better than their homogeneous analogues due to the unique structures formed on the surfaces (40–48). These two techniques, metal-complex attachment on oxide surfaces and subsequent molecular imprinting at the surfaces, may provide a new way to design active and selective catalytic metal sites with template-imprinted spaces.

Recently, we succeeded in preparing and characterizing in detail a new molecular-imprinting Rh-dimer catalyst on a SiO_2 surface (49, 50). The bridged Rh dimer $Rh_2Cl_2(CO)_4$ used as precursor was attached to the SiO_2 (Ox.50) surface and the template ligand $P(OCH_3)_3$ was coordinated to the attached Rh dimer. An obtained Rh monomer pair with two template ligands per Rh atom was converted to a Rh-dimer structure again by surface imprinting with SiO_2-matrix overlayers formed by hydrolysis–polymerization of $Si(OCH_3)_4$ on the Ox.50 surface. Coordinatively unsaturated Rh dimers (Rh–Rh, 0.268 nm) with cavities of the template size in micropores 0.74 nm in diameter were produced by step-by-step preparation at the surface. Individual synthesis steps were characterized by FT-IR, XPS, elemental analysis, solid-state MAS NMR, BET, and EXAFS (49, 50). The imprinted Rh dimers were found to act as highly active catalysts for hydrogenation of 3-ethyl-2-pentene. The template ligand $P(OCH_3)_3$ was regarded as an analogue of a half-hydrogenated species of 3-ethyl-2-pentene.

In this paper, we report catalytic performances of the novel imprinted Rh dimer for hydrogenation of alkenes of different sizes and shapes. This new approach to selective catalysis on the imprinted Rh dimer is based on the following: (i) conformation of ligands on the Rh dimer, (ii) orientation of vacant sites (for adsorption and reaction) on the Rh dimer, (iii) cavity space with a template-molecular shape (reaction space), and (iv) architecture of the cavity wall. The molecular-imprinting Rh-dimer catalyst exhibited remarkable activity for alkene hydrogenation after the surface imprinting, as well as size and shape selectivities discriminating methyl and ethyl groups of alkenes.

EXPERIMENTAL

Catalyst Preparation

Catalyst preparation has been described in detail in a separate paper (49). The procedure of synthesis of the imprinted Rh dimer is briefly summarized. All solvents used in this study were purchased from WAKO chemicals (research grade) and used without further purification. SiO_2 (Ox.50, Degussa; surface area, 50 $m^2\ g^{-1}$) was preevacuated at 673 K for 1 h, then impregnated with an *n*-hexane solution of $Rh_2Cl_2(CO)_4$ (Aldrich) under nitrogen (99.999% purity) atmosphere, followed by evacuation to remove the solvent at room temperature. The obtained Rh sample is denoted $Rh_2Cl_2(CO)_4/SiO_2$.

A diethyl ether solution of $P(OCH_3)_3$ (four times more than the Rh quantity) was added to the $Rh_2Cl_2(CO)_4/SiO_2$ under nitrogen atmosphere. The mixture was stirred for 30 min at room temperature and then evacuated in vacuum. Further treatment at 363 K for 3 h in vacuum changed the color of the sample to bright yellow. The obtained sample is denoted supported Rh catalyst (Rh_{sup}). The Rh loading used in this study was 0.43 wt% Rh/SiO_2, which corresponds to 0.25 Rh dimers nm^{-2} at the Ox.50 surface.

Both $Si(OCH_3)_4$ (0.68 g per 1 g of Ox.50) and H_2O (0.34 g) were admitted to the Rh_{sup} catalyst placed in a closed batch reactor at room temperature, with a chemical vapor deposition (CVD) technique vaporizing them at 373 K. After CVD, the whole closed system was heated at 348 K for 7 h to promote the hydrolysis–polymerization of $Si(OCH_3)_4$ for surrounding the attached Rh complexes and then evacuated at 363 K for 12 h to remove a $P(OCH_3)_3$ ligand as template. The obtained sample is denoted imprinted Rh catalyst (Rh_{imp}). All catalysts were stored in Schlenk tubes under vacuum in a refrigerator until use.

H_2 Adsorption

The Rh_{imp} catalyst (700 mg) was enclosed in a closed system and preevacuated at room temperature for 1 h. The dead volume of the system (60 cm^3) was measured using helium gas at ambient temperature. Hydrogen adsorption was measured at room temperature in the pressure range 0–93 kPa. This manipulation was repeated three times for the same sample to estimate the amount of irreversible and reversible adsorption on the Rh dimer site.

EXAFS

The Rh_{imp} catalysts at each step of the hydrogenation of 3-methyl-2-pentene were characterized by EXAFS; the fresh Rh_{imp} catalyst, the catalyst after H_2 adsorption, and the H_2-adsorbed catalyst reacted with 3-methyl-2-pentene. The treatments of the EXAFS samples were carried out as follows. The Rh_{imp} catalyst was exposed to 101.3 kPa of H_2 at room temperature in a closed system. After 30 min, H_2 was evacuated at ambient temperature and the obtained sample (about 260 mg) was enclosed in an EXAFS cell (cross section, 12.56 mm^2) under N_2 atmosphere and stored in a refrigerator until EXAFS measurement. The H_2-adsorbed sample was exposed to 3-methyl-2-pentene vapor (three times more than the Rh quantity) at 348 K for 5 min for the hydrogenation. This reaction time corresponded to one turnover number (product molecule/Rh dimer). The sample was evacuated at 348 K for 1 h and enclosed in an EXAFS cell under N_2 atmosphere and stored until EXAFS measurement.

EXAFS spectra at the Rh K-edge were measured in a transmission mode at 15 K at the BL-10B station in the Photon Factory at the Institute of Materials Structure Science, High Energy Accelerator Research Organization (KEK-IMSS-PF) (Proposal 2001G315). The energy and current of electrons in the storage ring were 2.5 GeV and 250–400 mA, respectively. X-rays from the storage ring were monochromatized by a Si(311) channel-cut crystal. Ionization chambers filled with pure Ar and Kr gases were used to monitor the intensities of the incident and transmitted X-rays, respectively. The EXAFS spectra were analyzed by the UWXAFS package (51). The threshold energy E_0 was tentatively set at the inflection point of the absorption edge. The background was subtracted by the AUTOBK program. The k^3-weighted EXAFS data were Fourier transformed into R-space. The curve-fitting analysis was carried out using the FEFFIT program in the R-space. The k-range for the Fourier transformation and the fitting R-range were 30–140 nm^{-1} and 0.12–0.29 nm, respectively. The number of independent parameters (N_{ind}) in the curve fitting of the imprinted catalyst was evaluated to be 13 from the Nyquist law (52):

$$N_{idp} = 2\Delta k \Delta R \pi^{-1} + 2.$$

The fitting parameters were coordination numbers (CN), interatomic distances (R), Debye–Waller factors (σ), and a correction-of-edge energy (ΔE_0). The same ΔE_0 was used for all shells in a sample. Curve fitting of all samples was performed with three shells, Rh–O, Rh–P, and Rh–Rh, and the number of the fitting parameters for the imprinted catalyst was 10, which is smaller than the N_{idp}. The phase shift and backscattering amplitude for Rh–O, Rh–P, and Rh–Rh bonds were calculated by the FEFF8 code (53). The coefficient of the multiphoton effect (S_0^2) was fixed at 1.0 for the fitting.

^{29}Si Solid-State MAS NMR

The SiO_2-matrix overlayers in the Rh_{imp} catalyst and without the Rh dimers on Ox.50 were characterized by ^{29}Si solid-state MAS NMR. The sample without the Rh dimers was also prepared by CVD of $Si(OCH_3)_4$ and H_2O (the same quantities as those for the preparation of the Rh_{imp} catalyst) on Ox.50 preevacuated at 673 K for 1 h. All manipulations were same as those in the case of the Rh_{imp} catalyst except for Rh-complex attachment and $P(OCH_3)_3$ addition.

The ^{29}Si solid-state MAS NMR spectra were recorded on a Chemagnetics CMX-300 spectrometer operating at 59.68 MHz. A 5-mm-diameter zirconia rotor with kel-F caps was used. The MAS NMR spectra were measured by a single-pulse detection method with a pulse duration of 1.5 μs (corresponding to about $\pi/6$ pulse) in the hydrogen decoupling mode. The rotor spin rate was 4 kHz, with an acquisition interval of 20 s. Chemical shifts are given in parts per million relative to tetramethylsilane fused in a glass tube as external standard. $Si(OCH_3)_4$ solved in $CDCl_3$ was fused in a glass tube and also measured with the same spectrometer. Peak signals attributed to SiO_2-matrix overlayers in the imprinting catalysts were discriminated from those for SiO_2 (Ox.50) bulk by the following procedure. Peak areas of the samples depend on the amount of sample and the number of measurements accumulated. The linearity of the NMR peak areas for Ox.50 to its amount and the number of measurements accumulated were confirmed by plural NMR measurements for various amounts of Ox.50 with different accumulated numbers. The results gave a linear dependency of the peak area on the accumulated number for an equal amount of the samples. Error range was 4.2%. Then the peak signal of Ox.50 was calibrated using the accumulated number and the amount of Ox.50 per the total amount of SiO_2 overlayers and Ox.50. A calculated signal for Ox.50 was subtracted from the overall peak signals, including those for SiO_2 overlayers and Ox.50, and curve-fitting deconvolution of the obtained difference spectrum corresponding to SiO_2-matrix overlayers was carried out for Q_4, Q_3, and Q_2 species.

BET Analysis

Nitrogen (99.99995% purity) adsorption BET analysis was performed with a BELSORP 28SA apparatus. Samples (40–50 mg) were evacuated at 363 K for 5 h before the measurements. The total dead volume was determined with helium gas. Nitrogen isotherms were obtained with N_2 gas in the pressure range 0–101.3 kPa and analyzed by the t-method (54), using amorphous silica as a standard material.

Catalytic Hydrogenation of Alkenes

Eight alkenes (2-pentene, 3-methyl-2-pentene, 4-methyl-2-pentene, 3-ethyl-2-pentene, 4-methyl-2-hexene, 2,4,4-trimethyl-2-pentene, 2-octene, and 1-phenylpropene) were used for catalytic hydrogenation reactions to examine size and shape selectivities for the molecular-imprinting catalyst. All alkenes were purchased from Tokyo Kasei Kogyo and used without further purification. Each catalyst (50–200 mg) was suspended in toluene solution under 101.3 kPa of hydrogen in a closed batch reactor equipped with a mechanical stirrer. Alkene hydrogenation reactions were carried out at 293–353 K by addition of neat alkene to the suspension (Rh/alkene/toluene molar ratio = 1/1,000/23,000). The reactions were monitored by gas chromatographical analysis at an appropriate interval.

Modeling of the Imprinted Rh-Dimer Catalyst

Modeling of the imprinted Rh-dimer catalyst was performed based on the molecular mechanics (MM) using a commercially available modeling tool, Cerius 2.4.2

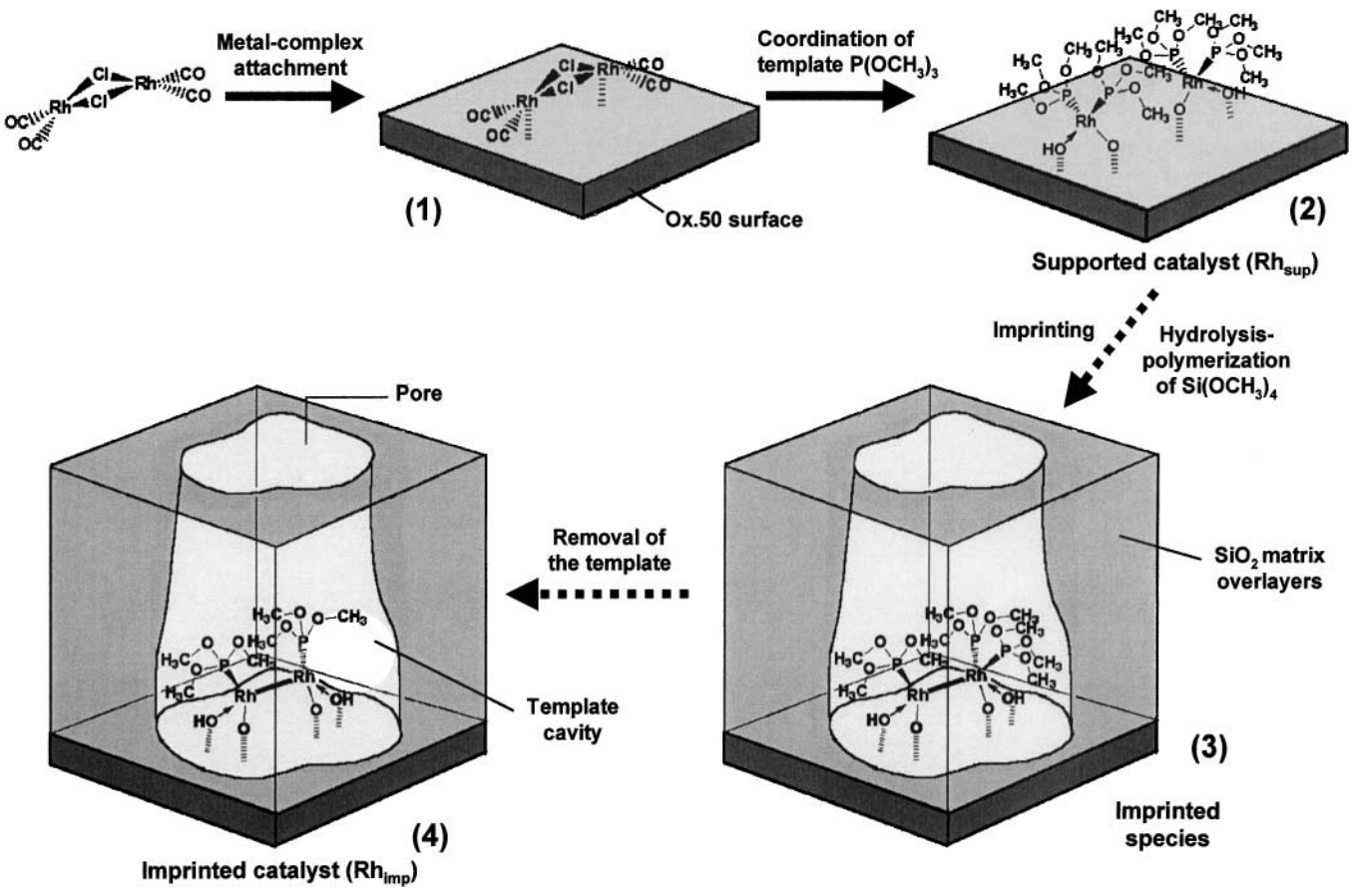

SCHEME 1. Preparation steps for the molecular-imprinting Rh-dimer catalyst by metal-complex attaching and imprinting on an Ox.50 surface.

(Accelrys), with the universal force field 1.02 (55, 56). The structure model of SiO_2-matrix overlayers and supported silica was taken from the database of the software for amorphous silica, and the structure was relaxed to minimize the total energy. Taking into account the structure of the imprinted Rh dimer determined by EXAFS and DFT calculation in our previous study (49, 50), we found that the imprinted structure was a Rh dimer which had one $P(OCH_3)_3$ ligand on a Rh atom and two $P(OCH_3)_3$ ligands on another Rh atom, as illustrated in Scheme 1 (imprinted species, (step 3). The Rh dimer with three $P(OCH_3)_3$ was placed in the middle of the silica matrix with the cubic size of $2.1 \times 2.1 \times 2.4$ nm^3. Si and O atoms were removed to form a pore, and silanol groups were formed at the wall surface of the pore so that the imprinting Rh dimer was located at the bottom of the pore in the SiO_2-matrix overlayers. Then, one of the two $P(OCH_3)_3$ ligands on a Rh atom was removed to leave the template cavity behind the $P(OCH_3)_3$ template, and the structure was optimized by MM. The structural parameters around the Rh atoms agreed with the EXAFS analysis within a deviation of 0.006–0.03 nm. Therefore the MM simulations were performed without any constraints.

RESULTS

EXAFS for the Imprinted Rh-dimer Catalyst

Structural parameters around Rh atoms in the Rh_{imp} catalyst at each step of the alkene hydrogenation were investigated by EXAFS. EXAFS spectra for three samples, fresh Rh_{imp} catalyst, Rh-dimer hydride species formed by adsorption of 101.3 kPa of H_2 at room temperature, and the sample after reaction of the hydride species with 3-methyl-2-pentene at 348 K for 5 min, were measured at 15 K.

Figure 1 shows k^3-weighted EXAFS oscillations and their associated Fourier transformed spectra at the Rh K-edge for the three samples. EXAFS analysis for the fresh Rh_{imp} catalyst was performed in the previous study (49, 50), and the determined structural parameters are given in Table 1. A proposed structure is illustrated in Scheme 1. EXAFS oscillation and Fourier transform of the Rh dimer after H_2 adsorption, shown in Figs. 1b and 1e, were similar to those shown in Figs. 1 a and 1d, respectively. The detailed analysis of the EXAFS data confirmed that the local conformation of the Rh dimer with a Rh–Rh bond (coordination number (CN), 1.3 ± 0.4), two Rh–O bonds (CN, 1.7 ± 0.5), and a Rh–P bond (CN, 1.2 ± 0.2) was retained after the

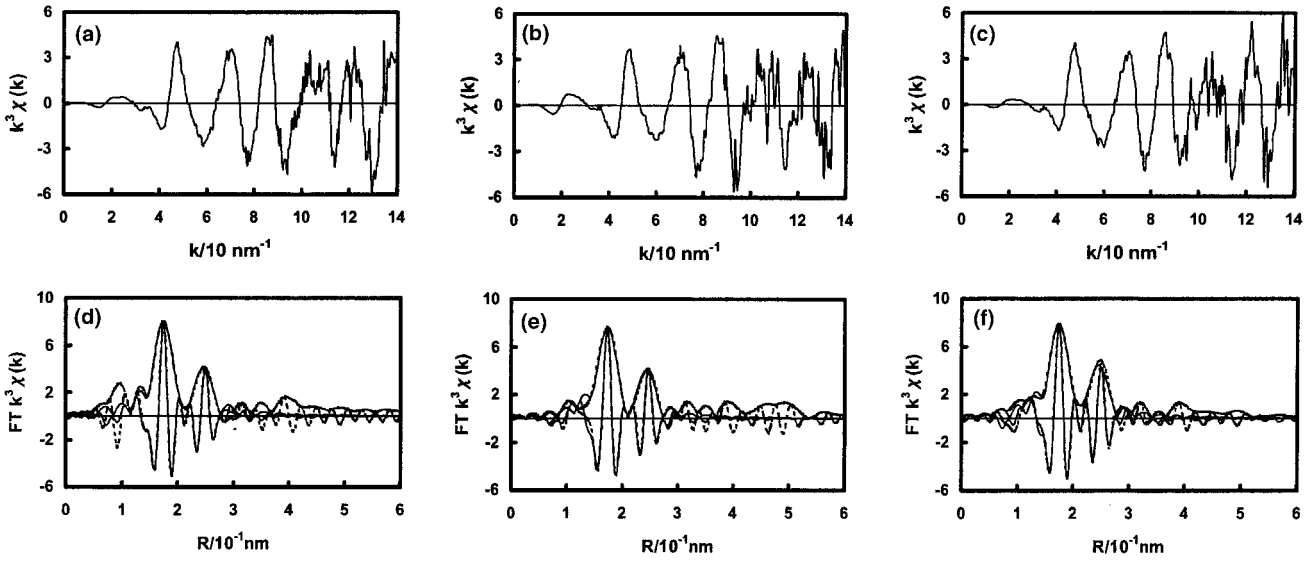

FIG. 1. k^3-weighted EXAFS oscillations (a–c) and their associated Fourier transforms (d–f) at the Rh K-edge measured at 15 K for the imprinted Rh_{imp} catalyst. Left (a, d), middle (b, e), and right (c, f) spectra are those for the fresh Rh_{imp} catalyst, the Rh_{imp} catalyst exposed to 101.3 kPa of H_2 at 293 K, and the Rh_{imp} catalyst after reaction of the H_2-exposed sample with 3-methyl-2-pentene at 348 K for 5 min, respectively. (Dotted and solid lines) The absolute values and imaginary parts of the observed data and the fitted spectra, respectively.

H_2 adsorption. But the distance between two adjacent Rh atoms changed from 0.268 to 0.265 nm. After reaction of the Rh-dimer hydride species with 3-methyl-2-pentene, the shortened Rh–Rh bond was recovered to the original bond length (0.270 ± 0.001 nm). Structural parameters for Rh–O and Rh–P were similar to those for the Rh_{imp} catalyst before H_2 adsorption. These results demonstrate that the Rh dimer structure is maintained at each step of the reaction sequences for the catalytic hydrogenation of 3-methyl-2-pentene.

H_2 Adsorption

Hydrogen adsorption measurements were performed three times at room temperature to examine the numbers of hydrogen adsorbed reversibly and irreversibly on the imprinted Rh dimer catalyst. Figure 2 shows the amount of H_2 adsorbed versus H_2 pressure. In the first run, the amount of adsorbed hydrogen increased with H_2 pressure and reached 1.22 H_2 per Rh dimer at saturation. In the second run after evacuation of the H_2-adsorbed sample at room temperature, only 0.32 H_2 per Rh dimer adsorbed. The same adsorption profile was observed in the third run, indicating reversible H_2 adsorption. Thus the majority of H_2 irreversibly adsorbed on the Rh dimers, and the number of H_2 molecules that adsorbed irreversibly was close to the number of Rh dimers.

^{29}Si Solid-State MAS NMR for SiO_2 Overlayers on Ox.50

Figure 3 shows ^{29}Si solid-state MAS NMR spectra for the Rh_{imp} catalyst with 4.7 SiO_2 monolayers, 4.7 SiO_2

TABLE 1

Structural Parameters Determined by EXAFS Curve-Fitting Analysis for the Imprinted Rh Catalysts Measured at 15 K

Shell	CN	R (nm)	σ^2 (nm^2)	
Fresh Rh_{imp} catalyst				$\Delta E_0 = 11 \pm 2$ eV
Rh–O	2.0 ± 0.5	0.211 ± 0.002	$(4 \pm 3) \times 10^{-5}$	$R_f = 0.3\%$
Rh–P	1.1 ± 0.2	0.221 ± 0.001	$(1 \pm 2) \times 10^{-5}$	
Rh–Rh	1.3 ± 0.3	0.268 ± 0.001	$(7 \pm 1) \times 10^{-5}$	
After H_2 adsorption				$\Delta E_0 = 9 \pm 4$ eV
Rh–O	1.7 ± 0.5	0.208 ± 0.003	$(6 \pm 3) \times 10^{-5}$	$R_f = 1.6\%$
Rh–P	1.2 ± 0.2	0.220 ± 0.001	$(2 \pm 4) \times 10^{-5}$	
Rh–Rh	1.3 ± 0.4	0.265 ± 0.001	$(7 \pm 2) \times 10^{-5}$	
After reaction of the H_2-adsorbed sample with 3-methyl-2-pentene				$\Delta E_0 = 12 \pm 3$ eV
Rh–O	2.2 ± 0.6	0.212 ± 0.003	$(5 \pm 4) \times 10^{-5}$	$R_f = 1.4\%$
Rh–P	1.1 ± 0.2	0.221 ± 0.001	$(1 \pm 4) \times 10^{-5}$	
Rh–Rh	1.2 ± 0.4	0.270 ± 0.001	$(6 \pm 2) \times 10^{-5}$	

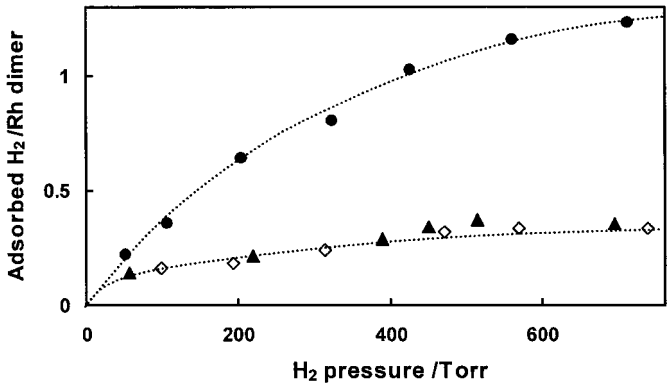

FIG. 2. Hydrogen adsorption on the imprinted Rh dimer catalyst at 293 K as a function of H_2 pressure. ●, ▲, and ◇ are the first, second, and third adsorption runs, respectively.

TABLE 2

^{29}Si MAS–NMR Measurements for SiO_2-Matrix Overlayers on Ox.50

Sample	Si(Q_2)	Si(Q_3)	Si(Q_4)
Rh_{imp} catalyst (4.7 ML)			
Chemical shift (ppm)	−92.5	−101.7	−110.7
Width[a]	3.7	5.8	4.6
Intensity[b]	0.156	0.616	0.206
SiO_2 overlayers without Rh complex (4.7 ML)			
Chemical shift (ppm)	—[c]	−102.2	−112.0
Width[a]	—[c]	4.4	7.1
Intensity[b]	—[c]	0.333	0.426

[a] Standard deviation.
[b] Normalized to the total area of supported material (Ox.50).
[c] Negligible.

monolayers on Ox.50 without the Rh complex, and Ox.50. Figure 3 also shows their difference spectra and the fitting deconvolution analysis. The observed three peaks are attributed to Q_4, Q_3, and Q_2 species for the surface SiO_2 matrices. Table 2 presents the analysis results for the two SiO_2-matrix overlayers. In both samples, the sharp peaks due to Q_4, Q_3 and Q_2 species were observed at similar chemical shifts. In the sample without Rh complex the Q_2 species with two silanol groups on a Si atom in the SiO_2-matrix overlayers was scarcely observed in Figs. 3c and 3d, while that for the Rh_{imp} catalyst corresponded to 16% of overall Si in the SiO_2-matrix overlayers as shown in Figs. 3a and 3b. Bulk Q_4 species of the Rh_{imp} catalyst was minor in Figs. 3a and 3b, while it was major in the SiO_2-matrix overlayers prepared without the Rh complex.

The catalyst weights increased after deposition of SiO_2-matrix overlayers by the hydrolysis–polymerization of

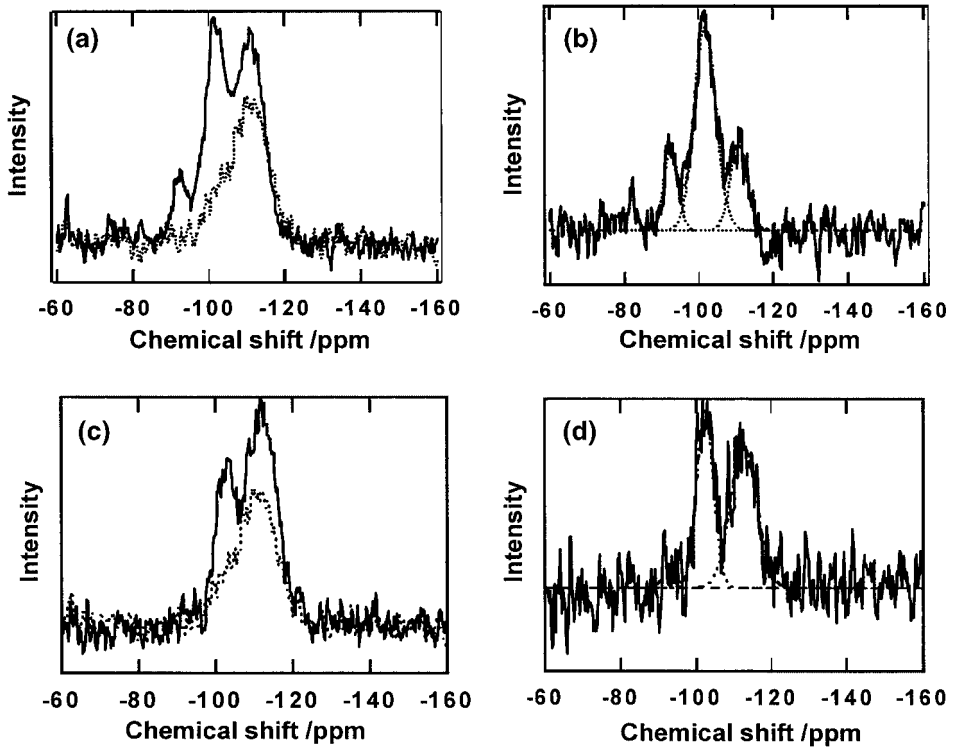

FIG. 3. ^{29}Si solid-state MAS NMR spectra for the Rh_{imp} catalyst with 4.7 SiO_2-matrix overlayers on Ox.50 (a) and for the same amount of SiO_2-matrix overlayers on Ox.50 without the template Rh complex (c). (Solid and dotted lines) The SiO_2-matrix overlayers + Ox.50 and Ox.50, respectively. (b, d) The difference spectra obtained by subtracting the Ox.50 spectrum (solid lines) and the curve-fitting deconvolution results, which are attributed to Q_4, Q_3, and Q_2 species of the SiO_2-matrix overlayers (dotted lines).

$Si(OCH_3)_4$. The weight gain indicated existence of physically adsorbed water in addition to the weight of the produced SiO_2 overlayers. To estimate the contribution of adsorbed water to the weight increase, the imprinted catalyst was evacuated at 363, 423, 523, and 673 K. It was estimated from extrapolation of the weights of the samples evacuated at the high temperatures to the value at 363 K that 84% of the amount of $Si(OCH_3)_4$ employed in the catalyst preparation was hydrolyzed. Assuming a cristobalite structure and taking into account the surface area of 50 m^2 g^{-1} for Ox.50, the amount of the SiO_2-matrix overlayers was estimated to be 4.7 monolayers 1.9 nm thick.

BET Analysis for Pore Size

BET analysis was performed to estimate whether micropores of the template were formed by the imprinting at the surface. Figures 4a and 4b are nitrogen adsorption isotherms for the Rh_{imp} catalyst and the SiO_2-matrix overlayers without the Rh complex template, respectively. Their *t*-plots are shown in Fig. 4c. Total surface areas of the two SiO_2-matrix overlayers increased compared with the Ox.50 support. There is a break at 0.37 nm in the *t*-plot for the Rh_{imp} catalyst. The break reveals formation of micropores 0.74 nm in diameter by the surface molecular imprinting. The pore size was somewhat smaller than the size of the imprinted Rh-complex intermediate with three $P(OCH_3)_3$ ligands shown in Scheme 1, which was estimated from the cross section of the intermediate calculated by DFT.

Catalytic Hydrogenation of Alkenes

The template ligand $P(OCH_3)_3$ has a shape similar to that of a half-hydrogenated species of 3-ethyl-2-pentene. To examine size and shape selectivities resulting from the molecular imprinting, eight alkenes, including 3-ethyl-2-pentene, were used as reactants for catalytic hydrogenation. Table 3 shows steady-state reaction rates (turnover frequencies (TOF)) of the hydrogenation of eight alkenes at 348 K on $Rh_2Cl_2(CO)_4$ (homogeneous system), $RhCl(P(OCH_3)_3)_3$ (homogeneous system), $Rh_2Cl_2(CO)_4$

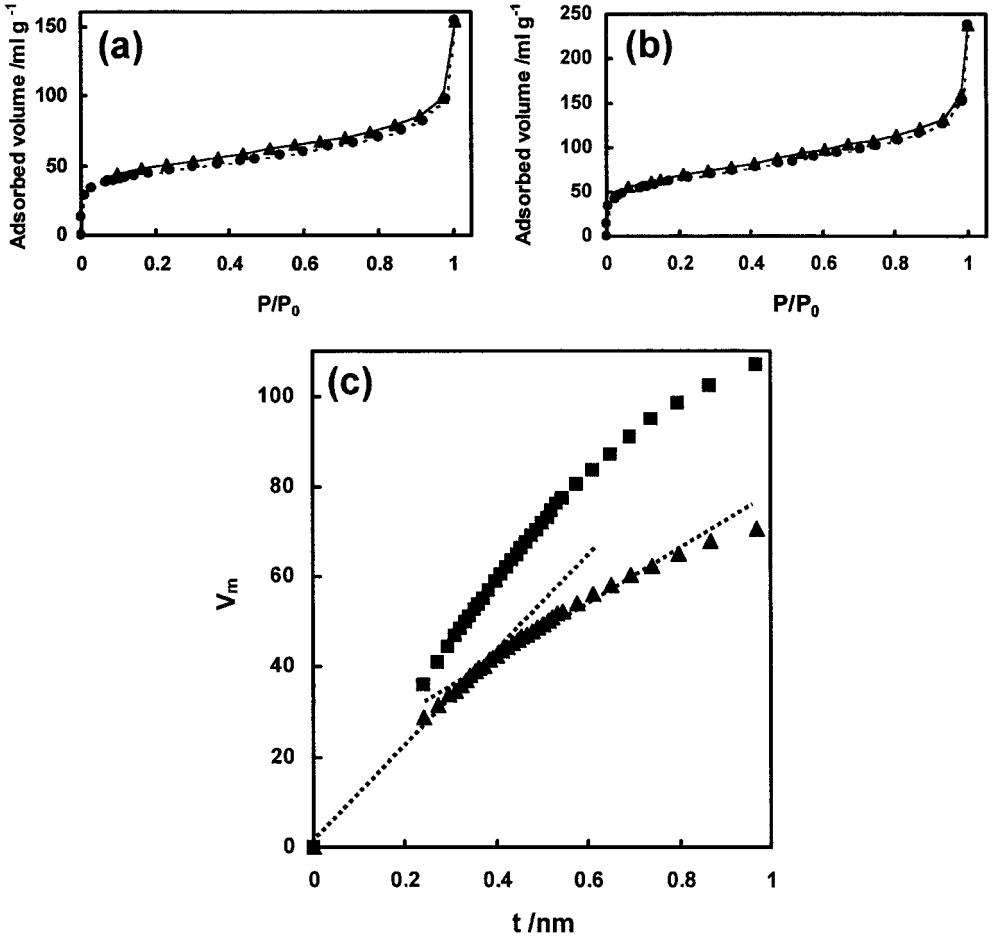

FIG. 4. Nitrogen adsorption isotherms for BET analysis at 77 K for the Rh_{imp} catalyst (a) and the SiO_2-matrix overlayers on Ox.50 without the Rh complex (b). (Dotted and solid lines) Adsorption and desorption of nitrogen, respectively. (c) The *t*-plots for the Rh_{imp} catalyst (▲) and the SiO_2-matrix overlayers on Ox.50 without the Rh complex (■).

TABLE 3

Steady-State Catalytic Activities (TOF s^{-1}) of the Rh Catalysts for Hydrogenation of Eight Alkenes under 101.3 kPa of H_2 in Toluene Solution[a]

Catalyst	$Rh_2Cl_2(CO)_4$[b]	$Rh_2Cl_2(CO)_4/SiO_2$	$RhCl(P(OCH_3)_3)_3$	Rh_{sup} catalyst	Rh_{imp} catalyst
2-Pentene	—	—	—	1.3×10^{-3}	6.6×10^{-2}
3-Methyl-2-pentene	—	—	—	7.0×10^{-5}	3.6×10^{-3}
4-Methyl-2-pentene	—	—	—	1.3×10^{-4}	5.9×10^{-3}
3-ethyl-2-pentene	0[c]	0[c]	0	4.4×10^{-5}	1.5×10^{-3}
2,4,4-Trimethyl-2-pentene	—	—	—	0	1.3×10^{-4}
4-Methyl-2-hexene	0[c]	0[c]	0	6.8×10^{-5}	9.6×10^{-4}
2-Octene	0[c]	0[c]	0	3.0×10^{-3}	3.0×10^{-2}
1-Phenylpropene	—	—	—	2.8×10^{-3}	2.0×10^{-2}

[a] Rh/alkene/toluene = 1/1,000/23,000 (molar ratio).
[b] Homogeneous system.
[c] Decomposition of Rh complex was observed.

attached on SiO_2 ($Rh_2Cl_2(CO)_4/SiO_2$), the supported Rh-complex catalyst (Rh_{sup}), and the molecular-imprinting catalyst (Rh_{imp}). The homogeneous catalysts $Rh_2Cl_2(CO)_4$ and $RhCl(P(OCH_3)_3)_3$ and the attached $Rh_2Cl_2(CO)_4/SiO_2$ catalyst showed no activity during the reaction. On the other hand, the Rh_{sup} catalyst exhibited significant catalytic activity under similar reaction conditions. It is to be noted that the hydrogenation reactions were remarkably promoted for all alkenes after the surface imprinting. It was found that the attached Rh structure changed from a monomer pair to a dimer with a Rh–Rh bond of 0.268 nm by the imprinting (49, 50).

The Rh_{imp} catalyst was highly active as well as so durable that it could be used repeatedly in toluene solution, as shown in Fig. 5. Figure 5 shows turnover number (TON) for the hydrogenation of 3-ethyl-2-pentene on the Rh_{sup} catalyst and the Rh_{imp} catalyst as a function of reaction time. The catalytic hydrogenation proceeded linearly on the both catalysts and such linearities in the performance were observed for all alkenes employed in this study, indicating high durability of the catalyst. Indeed, the second run reproduced the performance of the first run without any loss of catalytic activity, as shown in Fig. 5. The active Rh_{imp} catalyst was also air stable, which is advantageous in practical handling of the system.

The TOFs for the alkene hydrogenation on the Rh catalysts remarkably depended on the nature of the alkenes, as shown in Fig. 6 and Table 3. This was observed more or less on both Rh_{sup} and Rh_{imp} catalysts. The reaction rates were tremendously promoted after the surface molecular imprinting, but the degrees of increase for the alkenes were different from each other. Figure 7 shows the ratios of TOFs (TOF of the Rh_{imp} catalyst to TOF of the Rh_{sup} catalyst) for each alkene. The reactions of 2-pentene and 3-methyl-2-pentene, which are smaller molecules than the template $P(OCH_3)_3$, were promoted 51 times by the imprinting, as shown in Table 4 and Fig. 7. For 4-methyl-2-pentene, which is an isomer of 3-methyl-2-pentene, the hydrogenation was 45 times promoted. The hydrogenation of 3-ethyl-2-pentene whose half-hydrogenated species has

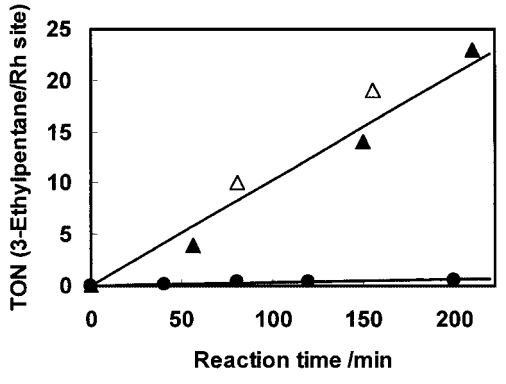

FIG. 5. TONs (turnover numbers) for hydrogenation of 3-ethyl-2-pentene at 348 K on the Rh_{sup} catalyst (●) and the Rh_{imp} catalyst (▲, first run : △, second run).

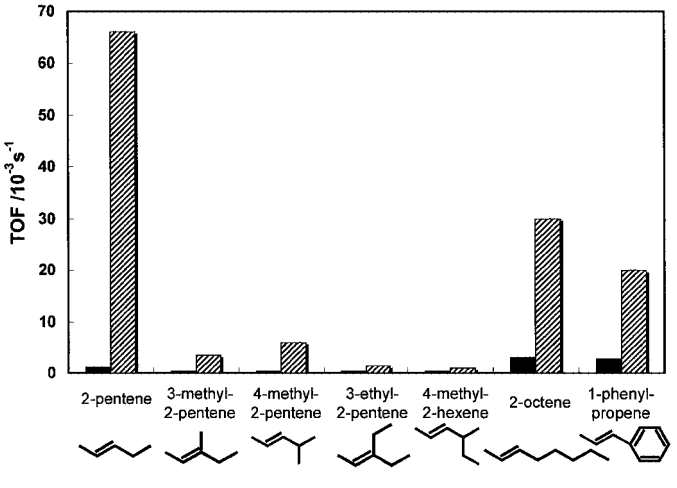

FIG. 6. TOFs (turnover frequencies) for hydrogenation of seven alkenes at 348 K on the Rh_{sup} catalyst (black) and the Rh_{imp} catalyst (slash).

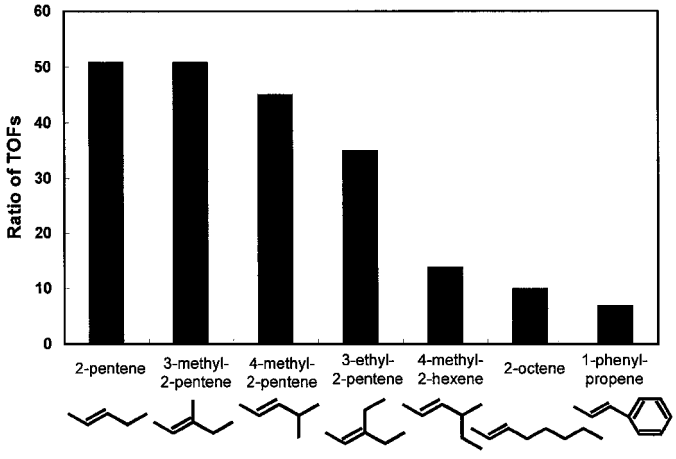

FIG. 7. Degree of enhancement of the reaction rates (ratio of TOFs) for seven alkenes as a result of surface molecular imprinting. The ratio of TOFs is that of the Rh_{imp} catalyst to that of the Rh_{sup} catalyst for each alkene.

a shape similar to that of the template was 35 times promoted. On the other hand, the enhancements for alkenes larger than 3-ethyl-2-pentene, such as 2-octene and 1-phenylpropene, were factors of 10 and 7, respectively, which were much less than those for the four left alkenes in Fig. 7. The promotion ratio for 4-methl-2-hexene, which is an isomer of 3-ethyl-2-pentene, was 14, which was much smaller than 35 for 3-ethyl-2-pentene.

To understand the different kinetic features in Figs. 6 and 7, activation energies and activation entropies for the catalytic hydrogenation of the alkenes on the Rh_{sup} catalyst and the Rh_{imp} catalyst were obtained in the temperature range 293–353 K. The kinetic parameters determined for seven alkenes are shown in Table 4. Activation enthalpies at 348 K are also given in Table 4, which are different by RT (T, 348 K) from the corresponding activation energies. Activation energies for hydrogenation on the Rh_{sup} catalyst were divided into values of approximately 30 and 42 kJ mol^{-1} for the linear alkenes, such as 2-pentene, 2-octene, and 1-phenylpropene, and the branch alkenes, respectively. Such a large difference in activation energy was also observed with Wilkinson complex. In contrast, activation entropies for hydrogenation on the Rh_{sup} catalyst were similar to each other: the values were in the range −200 to −215 J mol^{-1} K^{-1} for all alkenes.

After the imprinting, significant differences between small and large alkenes were observed in both activation energy and activation entropy. The activation energies for the hydrogenation of 3-ethyl-2-pentene and for alkenes smaller than 3-ethyl-2-pentene (four left alkenes in Fig. 7) on the Rh_{imp} catalyst were 26–43 kJ mol^{-1}, values similar to those observed on the Rh_{sup} catalyst. The activation entropies for the four alkenes were −170 to −195 J mol^{-1} K^{-1}, which were larger than those (−200 to −210 J mol^{-1} K^{-1}) obtained for the Rh_{sup} catalyst (Table 4). In contrast, for the larger alkenes, such as 4-methyl-2-hexene, 2-octene, and 1-phenylpropene, the activation energies were 10, 7, and 8 kJ mol^{-1}, respectively, very small values compared with those for the Rh_{sup} catalyst and other metal complex catalysts. Furthermore, the activation entropies reduced significantly, from about −210 to about −260 J mol^{-1} K^{-1}, as shown in Table 4. The conspicuous changes in kinetic parameters for the larger alkenes paralleled the changes in enhancement of the reaction rates, as shown in Table 4 and Fig. 7.

DISCUSSION

Structures of the Imprinted Rh Dimers after H_2 Adsorption and Alkene Hydrogenation

The new molecular-imprinting Rh-dimer catalyst (Rh_{imp}) with a Rh–Rh bond at a distance of 0.268 nm was much more

TABLE 4

Degrees of Enhancement of the Reaction Rates by Molecular Imprinting (Ratio of TOFs), Activation Energies (E_a), Activation Enthalpies ($\Delta^{\ddagger}H$), and Activation Entropies ($\Delta^{\ddagger}S$) for the Catalytic Hydrogenation of Alkenes at 348 K

Reactant	Supported catalyst (Rh_{sup})			Imprinted catalyst (Rh_{imp})			Ratio of TOFs[d]
	E_a[a]	$\Delta^{\ddagger}H$[b]	$\Delta^{\ddagger}S$[c]	E_a[a]	$\Delta^{\ddagger}H$[b]	$\Delta^{\ddagger}S$[c]	
2-Pentene	34	31	−205	26	23	−195	51
3-Methyl-2-pentene	44	41	−200	43	40	−170	51
4-Methyl-2-pentene	40	37	−207	40	37	−175	45
3-Ethyl-2-pentene	42	39	−210	39	36	−189	35
4-Methyl-2-hexene	40	37	−212	10	7	−276	14
2-Octene	28	25	−215	7	4	−257	10
1-Phenylpropene	29	26	−213	8	5	−256	7

[a] E_a: kJ mol^{-1}.
[b] $\Delta^{\ddagger}H$: kJ mol^{-1}.
[c] $\Delta^{\ddagger}S$: J K^{-1} mol^{-1}.
[d] Ratio of TOFs: TOF of the Rh_{imp} catalyst/TOF of the Rh_{sup} catalyst.

active than the supported Rh catalyst (Rh_{sup}) for the alkene hydrogenation, as shown in Fig. 6. The coordinatively unsaturated Rh dimers were stable under the reaction conditions, as shown in Fig. 5, which depicted durability for reuse as catalyst. In contrast, in homogeneous systems, such active unsaturated Rh species often decompose to form dimer species during catalytic cycles, and the dimer species in solution seldom work as catalysts (57). Therefore, first we investigated whether the Rh_{imp} catalyst held the dimer structure during the course of alkene hydrogenation by EXAFS and H_2 adsorption.

The Rh_{imp} catalyst was prepared as illustrated in Scheme 1 (49, 50). The Rh species at each step were characterized by EXAFS, XPS, FT-IR, and ICP(49, 50). One Rh site in the dimer (Rh_{imp}) possesses a template cavity as reaction site, and the other does not have the cavity near the site (step 4 in Scheme 1). This structure is derived from the intermediate species [$Rh(P(OCH_3)_3)$–$Rh(P(OCH_3)_3)_2$] (step 3 in Scheme 1), which is surrounded by SiO_2-matrix overlayers on an Ox.50 surface. The species (step 3) has been demonstrated by DFT calculation in a previous study (49). A $P(OCH_3)_3$ ligand, was desorbed to leave the cavity behind the template ligand, as shown in step 4 of Scheme 1.

These Rh sites have only four bonds per Rh, including a Rh–Rh bond at 0.268 nm, as shown in Table 1. The Rh_{imp} catalyst was exposed to H_2 at room temperature to form a Rh-hydride species. There are two possibilities for the hydride complex, which is a first intermediate of catalytic alkene hydrogenation cycle: one is monohydride and the other is dihydride. From the results of the H_2 adsorption shown in Fig. 2, the number of H_2 adsorbed per Rh dimer was 1.25 at saturation, which excludes the possibility of dihydride formation on both Rh sites of the dimer. Thus it is suggested that H_2 adsorbs dissociatively to form Rh-monohydride complexes. One might indicate the possible formation of a $Rh(H)_2$–Rh pair, but this is much less plausible because (i) there is no reason for discriminating between the two Rh sites for adsorption of small H atoms, and (ii) the Rh atom without hydrides has a four-coordination structure, on which H_2 should also adsorb eventually to form a $Rh(H)_2$–$Rh(H)_2$ pair, which is not the case experimentally.

The adsorption of hydrogen to produce the monohydride species was irreversible, as shown in Fig. 2. The second and third runs coincided with each other, which demonstrates the existence of reversible H_2 adsorption. By subtracting the reversible H_2 adsorption from the total H_2 adsorption, the amount of irreversible H_2 adsorption was estimated to be 0.92 H_2/Rh dimer. Thus, most of the Rh sites in the Rh_{imp} catalyst are converted to have monohydride ligand at saturation of H_2 adsorption.

Because the monohydride complex could maintain the hydride ligand under vacuum, fortunately, structural parameters for the Rh complex, which were determined by EXAFS measured at 15 K (Fig. 1) were equal to those for the Rh complex *in situ* under H_2 atmosphere. Contraction of the Rh–Rh bond from 0.268 (±0.001) to 0.265 nm (±0.001 nm) was found with the hydride dimer, which indicates stabilization of the dimer structure by electronic rearrangement due to hydride coordination on both Rh atoms in the dimer. The shrunk Rh–Rh bond of the monohydride species expanded again to recover the initial bond length (0.270 ± 0.001 nm) after reaction with 3-methyl-2-pentene at 348 K, as shown in Table 1. During the hydrogenation process, the Rh–Rh bond was retained without breaking. Further, the bond distances and coordination numbers for Rh–O and Rh–P did not change significantly (Table 1). The EXAFS analysis demonstrates that alkene hydrogenation on the molecular-imprinting Rh_{imp} catalyst proceeds on the Rh-dimer unit in each step of the catalytic cycle. The Rh dimers are attached on the Ox.50 surface through the Rh–O interface bonding at 0.211 nm (±0.002 nm) and also surrounded by SiO_2-matrix overlayers.

SiO_2-Matrix Overlayers on an Ox.50 Surface

SiO_2-matrix overlayers formed on an Ox.50 surface by the CVD method were characterized by ^{29}Si solid-state MAS NMR (Fig. 3 and Table 2). Micropores formed in the SiO_2-matrix overlayers in which the Rh dimers were located were also characterized by BET analysis (Fig. 4). The ^{29}Si solid-state MAS NMR spectrum for the SiO_2-matrix overlayers was much different from that for the Ox.50 silica bulk, as shown in Figs. 3a and 3b. Three sharp peaks, at −111, −102, and −93 ppm, were assigned to Q_4 species ($Si(OSi)_4$), Q_3 species ($Si(OSi)_3$), and Q_2 species ($Si(OSi)_2$). The Q_4, Q_3, and Q_2 species may be regarded as a bulk Si–O–Si network, a surface monohydroxylated Si species, and a surface dihydroxylated Si species, respectively. The same amount of SiO_2-matrix overlayers as used for the Rh_{imp} catalyst were prepared without the Rh complex at the surface. The relative ratio of the bulk and surface Si species in Figs. 3c and 3d was much different from that for the Rh_{imp} catalyst (Figs. 3a and 3b). Of the total Si in the overlayers for the Rh_{imp} catalyst, 79% was surface species, while in the case of SiO_2-matrix overlayers prepared without the Rh complex, bulk Q_4 species was the major species and Q_2 species was negligible. The difference in the ^{29}Si solid-state MAS NMR between the two samples was caused by the presence of Rh dimers in micropores of the SiO_2-matrix overlayers of one and not the other. On the other hand, the chemical shifts were similar to each other, which indicates similar bond conformations for the polymerized silicas in the two samples.

A significant difference between the two samples was also observed in BET analysis. The SiO_2-matrix overlayers/Ox.50 sample without the Rh complex showed a typical BET curve for porous materials with nonuniform pores (Fig. 4). In contrast, there was a break at 0.37 nm in the *t*-plot for the Rh_{imp} catalyst, as shown in Fig. 4c, which

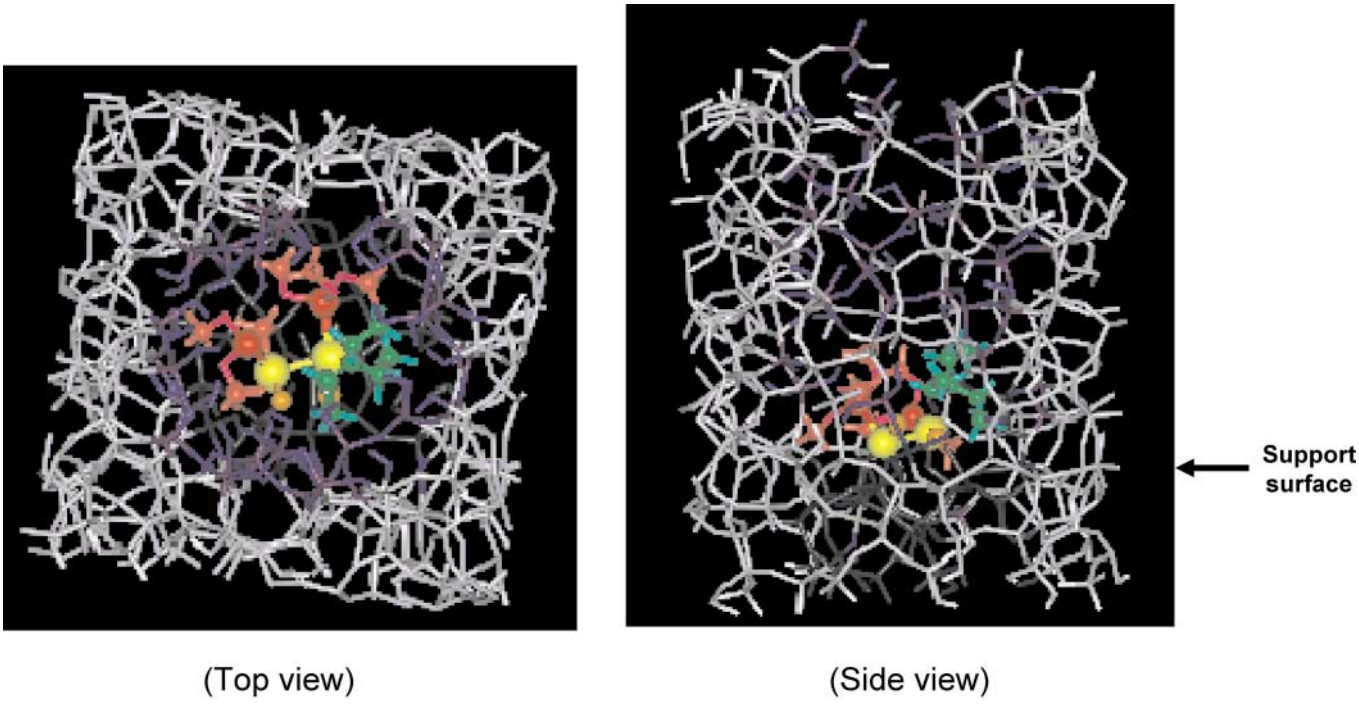

FIG. 8. Modeling of the imprinted Rh_{imp} catalyst coordinated with 3-ethyl-2-pentene by the MM method.

indicates the existence of uniform micropores 0.74 nm in diameter in the SiO_2-matrix overlayers.

These characterizations reveal that the SiO_2-matrix overlayers were formed on the Ox.50 surface by the hydrolysis–polymerization of $Si(OCH_3)_4$, surrounding the Rh dimers chemically attached on the surface to produce micropores 0.74 nm in diameter, as illustrated in Scheme 1. The cavity created behind the removed template ligand is also depicted in Scheme 1. The pore size agrees with the size of the Rh_{imp} catalyst estimated by MM calculation. The modeling of the Rh_{imp} dimer coordinated with the 3-ethyl-2-pentene located at the bottom of the pore is presented in Fig. 8.

Size and Shape Selectivities in Catalytic Hydrogenation of Alkenes

It was found that the catalytic activity of the supported Rh species for hydrogenation of alkenes was tremendously promoted (7–51 times) after the surface imprinting, as shown in Fig. 6 and Table 3. In contrast to the supported Rh_{sup} catalyst and the imprinted Rh_{imp} catalyst, $Rh_2Cl_2(CO)_4$ and its supported species $Rh_2Cl_2(CO)_4/SiO_2$ showed no activity for the hydrogenation reactions because these Rh complexes decomposed readily under the hydrogenation conditions. Coordination of $P(OCH_3)_3$ to the inactive $Rh_2Cl_2(CO)_4/SiO_2$ induced the activity of the Rh_{sup} catalyst, but a homogeneous complex $RhCl(P(OCH_3)_3)_3$ was inactive (Table 3). The Rh_{sup} monomer pairs are attached to the Ox.50 surface through Rh–O bonding at 0.203 nm (49, 50), which may modify the electronic state of the Rh center. The molecular imprinting created a new Rh-dimer structure with a Rh–Rh bond at 0.268 nm in the 0.74-nm pores of the SiO_2-matrix overlayers. The metal–metal bonding and coordinative unsaturation of the Rh dimer are key factors in the tremendous activity of the Rh_{imp} catalyst. The Rh dimers are also attached to the Ox.50 surface through an Rh–O bond at 0.211 nm (Table 1). It seems that the chemical attachment in a tetradentate form and the location with stable fitting in the micropore 1.9 nm thick prevented leaching of the Rh dimers to the reaction solution and decomposing and gathering of the Rh dimers.

Large ligands of metal complexes can regulate the reactivity of metal center electronically and geometrically to give higher selectivity than do metal and metal oxide catalysts without ligands. Surface-attached metal complexes are also subjected to regulation by the surface, which is regarded as a unique and large ligand. Indeed, the Rh_{sup} catalyst showed remarkable selectivity for the alkene hydrogenation, as shown in Fig. 6. The hydrogenation rate of 2-pentene on the Rh_{sup} catalyst was 19 times faster than those of 3-methyl-2-pentene and 4-methyl-2-pentene, which have methyl groups at the 3- and 4-carbon positions, respectively. In contrast to the branch alkenes, the length of the alkene main chain did not negatively affect the reaction rate (see, for example, 2-pentene, 2-octene, and 1-phenylpropene, as shown in Fig. 6 and Table 3).

Selectivity for the alkene hydrogenation on the Rh_{imp} catalyst is more complicated. It depends on the size and

shape of the template cavity used as reaction site in the micropores of the SiO_2-matrix overlayers on the Ox.50 surface, in addition to the electronic and geometric effects of the ligands. To see the molecular-imprinting effect on selectivity, we calculated the ratio of the TOF of the Rh_{imp} catalyst to the TOF of the Rh_{sup} catalyst for each alkene. The TOF ratios reduced with an increase in alkene size as shown in Fig. 7. It is to be noted that there was a large decrease in the TOF ratios of 3-ethyl-2-pentene and 4-methyl-2-hexene. Since a half-hydrogenated species of 3-ethyl-2-pentene has a shape similar to the template ligand $P(OCH_3)_3$, the big difference in the rate enhancement is due to the difference in the shape of the alkenes. The difference in the TOF ratios between 4-methyl-2-pentene and 4-methyl-2-hexene was very large where the difference in the size of a methyl group is discriminated on the Rh_{imp} catalyst. The TOF ratio for 4-methyl-2-hexene was much smaller than that for 2-pentene, as shown in Fig. 7, where the difference in the alkenes is the size and shape of the ethyl group. There was also a big difference between TOF ratios for 2-pentene and 2-octene, where a propyl group could be discriminated. Thus, the molecular-imprinting catalyst discriminates the size and shape of the alkenes. However, there was no significant difference in the TOF ratios between 2-pentene and 4-methyl-2-pentene, between those of 3-methyl-2-pentene and 3-ethyl-2-pentene, and between those of 2-pentene and 3-ethyl-2-pentene, as shown in Fig. 7. Thus, the molecular-imprinting catalyst could not discriminate the existence of methyl and ethyl groups among alkenes smaller than the template size. It is noteworthy that the reaction rates of 2-pentene, 2-octene, and 1-phenylpropene on the Rh_{sup} catalyst were similar to each other, whereas the rate enhancements (TOF ratios) for 2-octene and 1-phenylpropene (10 and 7 times, respectively) were much less than that for 2-pentene (51 times). Because the length of the linear alkene chains could not be discerned by a ligand-coordinated metal site, it is supported that the difference was caused by a wall of the template cavity around the Rh dimer site.

Regulation of Alkene Hydrogenation on the Imprinted Rh-Dimer Catalyst

The mechanism for alkene hydrogenation on Rh-complex catalysts such as the Wilkinson complex $RhCl(PPh_3)_3$ has been demonstrated by careful kinetic (57–70) and spectroscopic (71, 72) studies. The well-known hydrogenation mechanism involves four steps: dissociation of hydrogen molecules on metal center to form hydrides, coordination of an alkene C=C double bond to the metal center, insertion to the Rh–H bond to form a half-hydrogenated alkyl species, and reaction of the alkyl with the remaining hydride. The rate-determining step has been experimentally considered to be the third step (formation of alkyl) and this suggestion was confirmed by ab initio MO calculation (73, 74). To understand the mechanism of regulation of the catalytic hydrogenation of alkenes on the Rh_{imp} catalyst, Arrhenius parameters for the alkene hydrogenation on the Rh_{sup} catalyst and Rh_{imp} catalyst were compared (Table 4).

Activation energies for alkene hydrogenation on the Rh_{sup} catalyst were classified into two values, ca. 30 and 42 kJ mol^{-1} for linear and branch alkenes, respectively. These are typical values for the activation energies on metal-complex catalysts such as the Wilkinson complex in homogeneous systems, where the rate-determining step is the formation of a half-hydrogenated alkyl intermediate by insertion of π-coordinated alkene to a Rh–H bond. The energy barrier for the formation of a half-hydrogenated intermediate increases with branch alkenes. On the other hand, activation entropies for the catalytic hydrogenation on the Rh_{sup} catalyst were similar for all the alkenes used in this study, which indicates that restriction of conformations in the transition states to form the half-hydrogenated species does not depend on the size and shape of alkene molecules in the case of the Rh_{sup} catalyst.

In addition to the change in the ratio of TOFs among the alkenes with different sizes and shapes (Fig. 7), kinetic parameters for the alkene hydrogenation on the Rh_{imp} catalyst changed particularly for the alkenes of larger size than and different shape from the template ligand $P(OCH_3)_3$, as shown in Table 4. Activation energies of alkenes smaller than 3-ethyl-2-pentene did not change significantly after the imprinting (Table 4). For these alkenes the ratios of TOFs were as large as 35–51. These results mean that the rate-determining step for the smaller alkenes does not change by imprinting and the hydrogenation of the smaller alkenes is not regulated by the cavity with the template shape. In contrast, activation energies for the larger and different-shape alkenes compared to the template (their TOF ratios were 7–14) were as small as 7–10 kJ mol^{-1}. These dramatic reductions in activation energy and TOF ratio can be explained by a shift in the rate-determining step from alkyl formation to coordination of alkene to the Rh site. Along with this shift, the activation entropies for those alkene molecules also decreased greatly, from about -180 to about -260 J mol^{-1} K^{-1} for the other small molecules. It suggests that conformation of the coordinated alkene in the template cavity is regulated by a wall of the cavity and remaining $P(OCH_3)_3$ ligands.

The narrow pore in the overlayers and the small space (template cavity) around the Rh site would disturb the approach of larger molecules to the Rh site due to steric hindrance. There was a large difference in both rate promotions and kinetic parameters between 3-ethyl-2-pentene and 4-methy-2-hexene, as shown in Table 4. The two molecules have similar sizes but shapes different from each other. The pore 0.74 nm in diameter in the imprinted Rh_{imp} catalyst is large enough for these alkenes to enter. Thus, for the alkenes with the larger sizes and different shapes

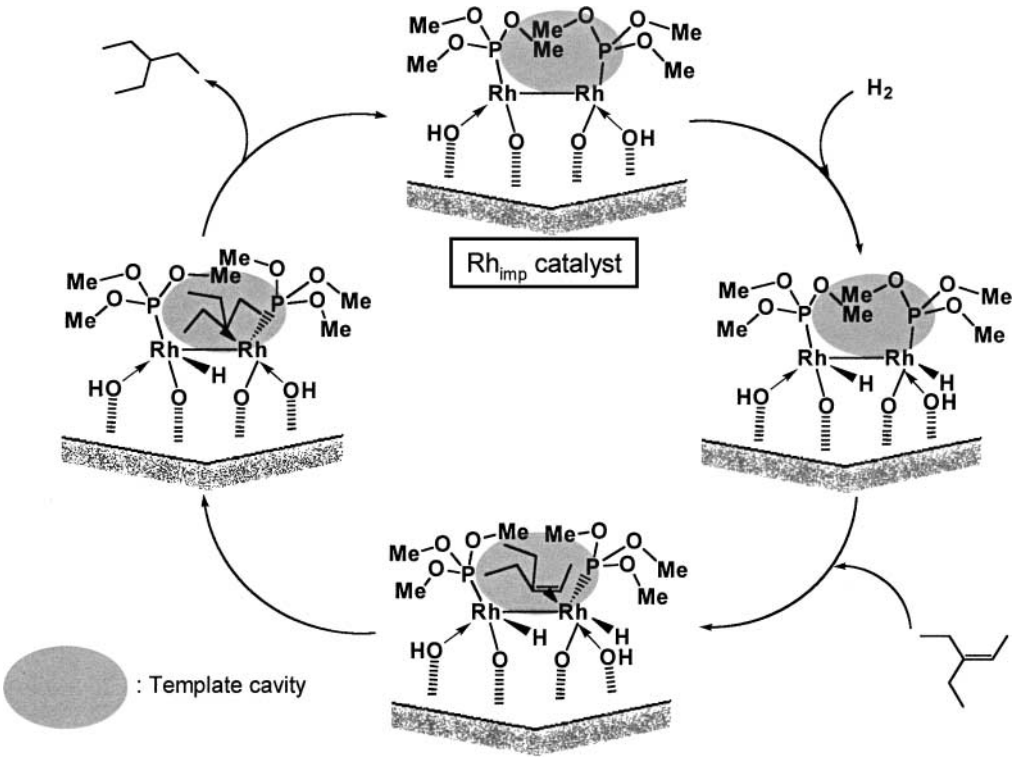

FIG. 9. The catalytic cycle of alkene hydrogenation on the imprinted Rh-dimer catalyst.

compared to the template, shown in Table 4 and Fig. 7, coordination of the alkenes to the Rh (steric hindrance in the template cavity around the Rh site) rather than diffusion of the alkenes in the micropore (steric hindrance in the pore) may be a key step to regulating catalytic reaction for the larger alkenes.

On the basis of the characterizations of the Rh_{imp} catalyst in this study as well as in the previous study (49, 50), and on the basis of the kinetic parameters for the alkene hydrogenation on both Rh_{imp} and Rh_{sup} catalysts, we summarize the catalytic alkene hydrogenation cycle on the Rh_{imp} catalyst in Fig. 9. The regulation of the alkene hydrogenation occurs at the step coordinating alkene to the imprinted Rh dimer, probably due to the different sizes and shapes of the alkenes sticking out of the template cavity. It is to be noted that the sizes and shapes of alkenes without any functional group were discriminated on the Rh_{imp} catalyst, where the molecular imprinting of an active metal complex on an oxide surface was successful for the first time. Achievement of more strict recognition of molecules needs further investigation, but the molecular imprinting at the surface may be a promising way to design new catalytic materials.

CONCLUSION

Performances of hydrogenation of alkenes without functional group on a new SiO_2-attached molecular-imprinting Rh-dimer catalyst (Rh_{imp}) were investigated. Hydrogen adsorption and EXAFS studies demonstrated that the imprinted Rh dimer maintained its dimer structure during the course of alkene hydrogenation. The BET analysis revealed the existence of micropores 0.74 nm in diameter which were created in SiO_2-matrix overlayers on an Ox.50 surface formed by hydrolysis–polymerization of $Si(OCH_3)_4$ characterized by ^{29}Si solid-state MAS NMR. In the sample without the template Rh complex, such micropores were not produced. The molecular-imprinting Rh_{imp} catalyst exhibited remarkable activities for the alkene hydrogenation compared with the supported Rh monomer pairs before the imprinting. The Rh_{imp} catalyst was air stable and could be reused without any loss of activity in spite of its coordinatively unsaturated structure, probably because of a tetradentate attaching mode through Rh–O bonding and the location of the dimer in the micropore of the SiO_2-matirx overlayers. In addition to enhancement of the activity and stability by the surface imprinting, significant selectivity was observed for alkenes of different sizes and shapes. The degree of the rate enhancement by the imprinting was suppressed for the alkenes with sizes larger than and shapes, different from those of 3-ethyl-2-pentene. A half-hydrogenated species of 3-ethyl-2-pentene is regarded to have size and shape similar to the template ligand $P(OCH_3)_3$. Further, for hydrogenation of those alkenes the activation energies and activation entropies remarkably decreased, compared with those for the other small alkenes.

The drastic change in the kinetic parameters was explained by a shift in the rate-determining step from the alkyl intermediate formation to the alkene coordination to Rh. The conformation of two $P(OCH_3)_3$ ligands, the location of Rh, to which the alkenes coordinate, and the spatial architecture of the wall of the pore may produce the template cavity which acts as the reaction space for the size- and shape-selective alkene hydrogenation. To our knowledge, the imprinted Rh-dimer is the first example of molecular imprinting of an active metal complex at an oxide surface, though molecular recognition of reactants with functional groups is a next stage of the study.

ACKNOWLEDGMENTS

The authors thank Dr. T. Shido for measurements of a part of the EXAFS spectra. The XAFS measurements were done with the approval of the Photon Factory advisory committee (PAC) (Proposal 2001G315).

REFERENCES

1. Brady, P. A., and Sanders, J. K. M., *Chem. Soc. Rev.* **26**, 327 (1997).
2. Ramstrom, O., and Ansell, R. J., *Chirality* **10**, 195 (1998).
3. Shea, K. J., *Trends Polym. Sci.* **2**, 166 (1994).
4. Mosbach, K., *Trends Biochem. Sci.* 9 (1994).
5. Wulff, G., *in* "Polymeric Reagents and Catalysis" (W. T. Ford, Ed.), p. 186. Am. Chem. Soc., Washington, DC, 1986.
6. Sherrington, D. C., *Chem. Commun.* 2275 (1998).
7. Davis, M. E., Katz, A., and Ahmad, W. R., *Chem. Mater.* **8**, 1820 (1996).
8. Whitcombe, M. J., Alexander, C., and Vulfson, E. N., *Synlett* **6**, 911 (2000).
9. Sellergren, B., *Angew. Chem. Int. Ed.* **39**, 1031 (2000).
10. Klein, J. U., Whitcombe, M. J., Mulholland, F., and Vulfson, E. N., *Angew. Chem. Int. Ed.* **38**, 2057 (1999).
11. Hart, B. R., Rush, D. J., and Shea, K. J., *J. Am. Chem. Soc.* **122**, 460 (2000).
12. Yilmaz, E., Haupt, K., and Mosbach, K., *Angew. Chem. Int. Ed.* **39**(12), 2115 (2000).
13. Khasawneh, M. A., Vallano, P. T., and Remcho, V. T., *J. Chromatogr. A* **922**(1–2), 87 (2001).
14. Sellergen, B., *J. Chromatogr. A* **906**(1–2), 227 (2001).
15. Mosbach, K., *Chem. Rev.* **100**, 2495 (2000).
16. Malitesta, C., Losito, I., and Zambonin, P. G., *Anal. Chem.* **71**(7), 1366 (1999).
17. Lai, E. P. C., Fafara, A., VanderNoot, V. A., Kono, M., and Polsky, B., *Can. J. Chem.* **76**(3), 265 (1998).
18. Ye, L., and Mosbach, K., *J. Am. Chem. Soc.* **123**, 2901 (2000).
19. Morihara, K., Takiguchi, M., and Shimada, T., *Bull. Chem. Soc. Jpn.* **67**, 1078 (1994).
20. Robinson, D. K., and Mosbach, K., *J. Chem. Soc. Chem. Commun.* 969 (1989).
21. Heilmann, J., and Maier, W. F., *Angew. Chem., Intl. Ed. Engl.* **33**, 471 (1994).
22. Beach, J. V., and Shea, K. J., *J. Am. Chem. Soc.* **116**, 379 (1994).
23. Wulff, G., *Angew. Chem. Int. Ed. Engl.* **34**, 1812 (1995).
24. Wulff, G., Gross, T., and Schonfeld, R., *Angew. Chem. Intl. Ed. Engl.* **36**, 1962 (1997).
25. Alexander, C., Smith, C. R., Whitcombe, M. J., and Vulfson, E. N., *J. Am. Chem. Soc.* **121**, 6640 (1999).
26. Strikovsky, A. G., Kasper, D., Grun, M., Green, B. S., Hradil, J., and Wulff, G., *J. Am. Chem. Soc.* **122**, 6295 (2000).
27. Sellergren, B., Karmalkar, R. N., and Shea, K. J., *J. Org. Chem.* **65**, 4009 (2000).
28. Katz, A., and Davis, M. E., *Nature* **403**, 286 (2000).
29. Matsui, J., Nicholls, I. A., Karube, I., and Mosbach, K., *J. Org. Chem.* **61**, 5414 (1996).
30. Santora, B. P., Larsen, A. O., and Garne, M. R., *Organometallics* **17**, 3138 (1998).
31. Locatelli, F., Gamez, P., and Lemaire, M., *J. Mol. Catal. A* **135**, 89 (1998).
32. Polborn, K., and Severin, K., *Chem. Eur. J.* **6**, 4604 (2000).
33. Polborn, K., and Severin, K., *Eur. J. Inorg. Chem.* 1687 (2000).
34. Cammidge, A. N., Baines, N. J., and Bellingham, R. K., *Chem. Commun.* 2588 (2001).
35. Krebs, J. F., and Borovik, A. S., *J. Am. Chem. Soc.* **117**, 10593 (1995).
36. Krebs, J. F., and Borovik, A. S., *Chem. Commun.* 553 (1998).
37. Brunkan, N. M., and Gagne, M. R., *J. Am. Chem. Soc.* **122**, 6217 (2000).
38. Tanimura, T., Katada, N., and Niwa, M., *Langmuir* **16**, 3858 (2000).
39. Markowitz, M. A., Kust, P. R., Deng, G., Schoen, P. E., Dordick, J. S., Clark, D. S., and Gaber, B. P., *Langmuir* **16**, 1759 (2000).
40. Iwasawa, Y., *Adv. Catal.* **35**, 187 (1987).
41. Izumi, Y., Chihara, H., Yamazaki, H., and Iwasawa, Y., *J. Phys. Chem.* **98**, 594 (1994).
42. Asakura, K., Bando, K. K., Iwasawa, Y., Arakawa, H., and Isobe, K., *J. Am. Chem. Soc.* **112**, 9096 (1990).
43. Bando, K. K., Asakura, K., Arakawa, H., Isobe, K., and Iwasawa, Y., *J. Phys. Chem.* **100**, 13636 (1996).
44. Iwasawa, Y., *Stud. Surf. Sci. Catal.* **101**, 21 (1996).
45. Iwasawa, Y., *Acc. Chem. Res.* **30**, 103 (1997).
46. Fukui, K., Sugiyama, S., and Iwasawa, Y., *Phys. Chem. Chem. Phys.* **3**, 3871 (2001).
47. Shido, T., Yamaguchi, A., Asakura, K., and Iwasawa, Y., *J. Mol. Catal. A* **163**, 67 (2000).
48. Asakura, K., Noguchi, Y., and Iwasawa, Y., *J. Phys. Chem. B* **103**(7), 1051 (1999).
49. Tada, M., Sasaki, T., Shido, T., and Iwasawa, Y., *Phys. Chem. Chem. Phys.*, submitted.
50. Tada, M., Sasaki, T., Shido, T., and Iwasawa, Y., *Shokubai* **44**(2), 89 (2002).
51. Stern, E. A., Newville, M., Ravel, B., Yacoby, Y., and Haskel, D., *Physica B* **208**, 117 (1995).
52. Stern, E. A., *Phys. Rev. B* **48**, 9825 (1993).
53. Ankudinov, A. L., Ravel, B., Rehr, J., and Conradson, S. D., *Phys. Rev. B* **58**, 7565 (1998).
54. de Boer, J. H., Lippens, B. C., Linsen, B. G., Broekhoff, J. C. P., van den Heuvel, A., and Osinga, Th. J., *J. Colloid Interface Sci.* **21**, 405 (1966).
55. Castonguay, L. A., and Rappe, A. K., *J. Am. Chem. Soc.* **114**, 5832 (1992).
56. Rappe, A. K., and Colwell, K. S., *Inorg. Chem.* **32**, 3438 (1993).
57. Montelatici, S., van der Ent, A., Osborn, J. A., and Wilkinson, G., *J. Chem. Soc. A* 1054 (1968).
58. Osborn, J. A., Jardine, F. H., Young, J. F., and Wilkinson, G., *J. Chem. Soc. A* 1711 (1966).
59. Jardine, F. H., Osborn, J. A., and Wilkinson, G., *J. Chem. Soc. A* 1574 (1967).
60. Halpern, J., and Wong, C. S., *J. Chem. Soc. Chem. Commun.* 629 (1973).
61. Halpern, J., Okamoto, T., and Zakhariev, A., *J. Mol. Catal.* **2**, 65 (1976).
62. Halpern, J., *Trans. Am. Crystallogr. Assoc.* **14**, 59 (1978).
63. Halpern, J., *Inorg. Chem. Acta* **50**, 11 (1981).
64. Halpern, J., and Okamoto, T., *Inorg. Chem. Acta* **89**, L53 (1984).

65. Ohtani, Y., Fujimoto, M., and Yamagishi, A., *Bull. Chem. Soc. Jpn.* **49**, 1871 (1976).
66. Ohtani, Y., Fujimoto, M., and Yamagishi, A., *Bull. Chem. Soc. Jpn.* **50**, 1453 (1977).
67. Ohtani, Y., Fujimoto, M., and Yamagishi, A., *Bull. Chem. Soc. Jpn.* **52**, 69 (1979).
68. Rousseau, C., Evrard, M., and Petit, H., *J. Mol. Catal.* **3**, 309 (1978).
69. Rousseau, C., Evrard, M., and Petit, H., *J. Mol. Catal.* **5**, 163 (1979).
70. Siegel, S., and Ohrt, D., *Inorg. Nucl. Chem. Lett.* **8**, 15 (1972).
71. Meakin, P., Jesson, J. P., and Tolman, C. A., *J. Am. Chem. Soc.* **94**, 3240 (1972).
72. Tolman, C. A., Meakin, P. Z., Lindner, D. L., and Jesson, J. P., *J. Am. Chem. Soc.* **96**, 2762 (1974).
73. Koga, N., Daniel, C., Han, J., Fu, X. Y., and Morokuma, K., *J. Am. Chem. Soc.* **109**, 3455 (1987).
74. Daniel, C., Koga, N., Han, J., Fu, X. Y., and Morokuma, K., *J. Am. Chem. Soc.* **110**, 3773 (1988).